Eur. Phys. J. B **32**, 81–86 (2003)
DOI: 10.1140/epjb/e2003-00076-8

THE EUROPEAN PHYSICAL JOURNAL B

Cluster Monte Carlo dynamics for the Ising model on fractal structures in dimensions between one and two

P. Monceau[1,2,a] and P.-Y. Hsiao[1]

[1] Laboratoire de physique théorique de la matière condensée, Pôle matière et systèmes complexes[b], Université Paris 7, case 7020, 2 place Jussieu, 75251 Paris Cedex 05, France
[2] Département de physique et modélisation, Université d'Evry-Val d'Essonne, Boulevard F. Mitterrand, 91025 Evry Cedex, France

Received 29 November 2002
Published online 14 March 2003 –

Abstract. We study the cluster size distributions generated by the Wolff algorithm in the framework of the Ising model on Sierpinski fractals with Hausdorff dimension D_f between 1 and 2. We show that these distributions exhibit a scaling property involving the magnetic exponent y_h associated with one of the eigendirection of the renormalization flows. We suggest that a single cluster tends to invade the whole lattice as D_f tends towards the lower critical dimension of the Ising model, namely 1. The autocorrelation times associated with the Wolff and Swendsen-Wang algorithms enable us to calculate dynamical exponents; the cluster algorithms are shown to be more efficient in reducing the critical slowing down when D_f is lowered.

PACS. 68.35.Rh Phase transitions and critical phenomena – 05.45.Df Fractals – 75.10.Hk Classical spin models – 75.40.Mg Numerical simulation studies – 89.75.Da Systems obeying scaling laws

1 Introduction

The early works dealing with magnetic phase transitions on fractals have been done at the beginning of the eighties by Gefen *et al.* [1]. Instead of the replication of an elementary cell by translation, these structures are constructed by iteration of a generating cell, whose details are hence present at many scales. Dealing with such systems, where the translation invariance is broken, is a difficult task and few analytical results are available. Moreover, it is well known that a Monte Carlo-like approach to the study of magnetic second order phase transitions comes up against the difficulty of critical slowing down: The divergence of the correlation length at the critical point affects the efficiency of Monte Carlo simulations in the critical region because successive configurations are generally strongly correlated [2]. The slowing down hinders the efficiency of the simulations, in the case of phase transitions on fractal structures, for two main reasons:

i) Reliable studies of the critical behavior require the simulation of very large lattices, where the underlying network must be self-similar over several scales.

ii) The increase in the sizes involved in a finite-size analysis is very fast, since they define a geometrical series for a given Hausdorff dimension.

At the end of the eighties, the mapping between the percolation transitions and the magnetic ones, discovered by Fortuin and Kasteleyn [3], led Swendsen and Wang [4] and Wolff [5] to develop algorithms able to reduce the critical slowing down. Instead of flipping randomly chosen spins as one should do in the case of the Metropolis algorithm, one constructs one (or many) cluster at each Monte Carlo step. The use of such algorithms, together with the histogram method [6,7] enabled to improve significantly the study of the problem we set out at the beginning of this introduction. In this way, simulations of the Ising phase transition on Sierpinski fractals have been recently carried out in several Hausdorff dimensions between 1 and 3 [8–11], more efficiently than before. Monceau *et al.* devoted a recent paper to a synthetic discussion of the whole set of results obtained from these simulations [12]. The most striking points are the following:

i) Evidence has been found for increasing scaling corrections when the fractal dimension tends towards the lower critical dimension of the Ising model [11], namely 1.

ii) Discrepancies between the calculated critical exponents and the predictions of ϵ expansions [13] have led to conclude that these exponents do not only depend upon the symmetry of the order parameter and the fractal dimension but also upon the topological features of the fractal. Hence, the universality does not work in fractal structures in a usual way; it is said to be weak [14,15].

The goal of the studies quoted above was to deal with the thermodynamical aspects of the phase transitions; few works have been devoted to a study of the critical slowing down on fractal structures. The dynamical aspects of

[a] e-mail: pmo@ccr.jussieu.fr
[b] FR2438 CNRS

Table 1. Values of the critical parameters for $SC(25,24)$ and $SC(9,8)$ recalled from reference [11].

Structure	D_f	T_C	γ/ν	β/ν	$D_f-\gamma/\nu$
$SC(25,24)$	1.9746	2.0660(15)	1.750(5)	0.1108(4)	0.2246(50)
$SC(9,8)$	1.8928	1.4795(5)	1.732(4)	0.075(10)	0.1608(40)

Table 2. Values of the mean cluster sizes $\langle s\rangle_k$ for the fractals $SC(25,24)$ and $SC(9,8)$ at the critical point for different iteration steps k.

Structure	$k=3$	$k=4$	$k=5$	$k=6$	$k=7$
$SC(25,24)$	5280(5)	88475(64)	1487722(2570)		
$SC(9,8)$		2629(2)	18054(10)	123418(51)	839247(812)

the Wolff algorithm and the associated cluster distributions have been investigated in the case of three different fractal dimensions between 2 and 3 [16], and the short time dynamics for a structure with a Hausdorff dimension close to 1.89 [17]. The purpose of this article is to study the Wolff cluster size distribution and the autocorrelation times associated with the Wolff and Swendsen-Wang cluster dynamics in the case of fractal dimensions between 1 and 2, where scaling corrections are more important than between 2 and 3.

The outline of this paper is the following: The Ising model on Sierpinski fractal is recalled in Section 2. The cluster distributions generated by the Wolff algorithm and their scaling properties are studied in Section 3. The autocorrelation times and dynamical exponents associated with the Wolff and Swendsen-Wang algorithms are investigated in Section 4.

2 The Ising model on Sierpinski fractals

The fractal structures we deal with are deterministic Sierpinski carpets embedded in a two-dimensional space. A generating cell denoted by $SC(l^2,N_{occ},1)$ is firstly constructed by dividing a square into l^2 subsquares and deleting (l^2-N_{occ}) among them in the center of the initial square. This process is iterated on the remaining subsquares k times. We call $SC(l^2,N_{occ},k)$ the lattice built up from a finite number k of iteration steps and $SC(l^2,N_{occ})$ the "true" fractal obtained in the thermodynamical limit, when k tends to infinity. Given a finite structure $SC(l^2,N_{occ},k)$, we call $L=l^k$ the size of the lattice and $N=(N_{occ})^k$ the number of elementary subsquares. An Ising spin is located in the center of each of them; the exchange interaction is ferromagnetic and restricted to the first neighbors. The Ising model exhibits a second order ferromagnetic transition on these fractals [14] and the Hausdorff dimension is defined as: $D_f=\ln(N_{occ})/\ln(l)$. For a given fractal $SC(l^2,N_{occ})$, we shall call T_C the critical temperature, β, γ, ν the critical exponents associated respectively with the magnetization, the zero field magnetic susceptibility χ, and the correlation length ξ.

According to the Wolff algorithm [5], we build up a single cluster of parallel spins at each Monte Carlo step n and we compute the total energy $E(n)$, the magnetization $M(n)$, and the size $s(n)$, namely the number of sites, of the generated cluster. In the case of the Swendsen-Wang algorithm [4], the maximum number of clusters are constructed at each Monte Carlo step n until the entire lattice has been visited and a spin $+1$ or -1 is randomly assigned to each cluster; we call $E(n)$ the total energy and $M(n)$ the magnetization calculated at each step. We denote $\langle E\rangle$ and $\langle|M|\rangle$ the thermodynamical averages calculated over the Monte Carlo run at a given temperature. The normalized magnetization autocorrelation function reads as:

$$C_M(n)=\frac{\langle|M(0)|\,|M(n)|\rangle-\langle|M|\rangle^2}{\langle M^2\rangle-\langle|M|\rangle^2} \tag{1}$$

where $\langle|M(0)|\,|M(n)|\rangle$ is the average of the energy pairs separated by n steps. The energy autocorrelation function $C_E(n)$ follows the same form, without the absolute values.

3 Wolff cluster size distribution

The thermodynamical aspects of the phase transitions have been investigated by Monceau *et al.* [11], in the cases of four centered Sierpinski carpets, namely $SC(25,24)$, $SC(9,8)$, $SC(16,12)$ and $SC(25,16)$, and by Carmona *et al.* [9] in the case of $SC(9,8)$ and $SC(16,12)$. Their results show that scaling corrections can strongly affect the finite size behavior of some thermodynamical quantities, especially when the fractal dimension is lowered from 2 to 1; the critical exponents and the critical temperature cannot always be calculated, but bounds can be provided. Moreover, the maxima of the susceptibility follow the power laws expected from the finite-size analysis $\chi^{\max}(L)\sim L^{\gamma/\nu}$ with a very good reliability, which enables to calculate precisely the ratio of exponents γ/ν. Since we focus on the cluster size distribution at the critical point, we will study $SC(25,24)$ and $SC(9,8)$, for which values of the critical temperature can be provided [11]. The critical parameters T_C, β/ν and γ/ν calculated from a finite-size scaling analysis are summarized in Table 1.

We studied first the evolution of the mean cluster size $\langle s\rangle_k$ with L at the critical temperature. In each case, 5 Monte Carlo runs of $N_S=10^6$ steps have been carried out at the critical temperature. The results are summarized in Table 2. Power law fits under the form $\langle s\rangle_k\sim L^{d_{fw}}$ are satisfied, which enables us to define the fractal dimensions

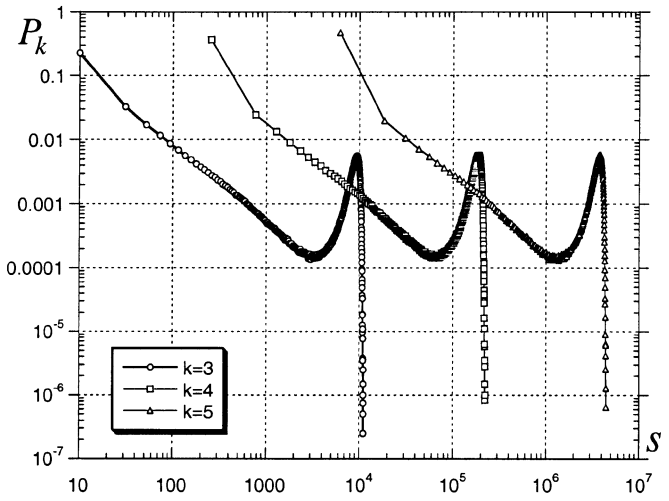

Fig. 1. Wolff cluster size distributions $P_k(s)$ for the fractal $SC(25,24)$ at three different iteration steps k. The histograms have been constructed with data obtained from 5×10^6 Monte Carlo steps at the critical temperature $T = 2.0660$ where 648 bins have been chosen. The values of the first bin are not meaningful because they are subject to large fluctuations.

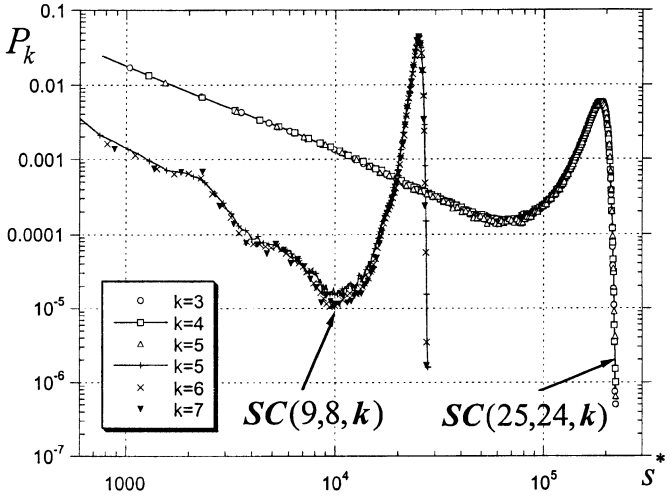

Fig. 2. Data collapses of the Wolff cluster size distributions P_k at the critical points. The cluster size has been rescaled, to show $P_3(s^*/l^x)$, $P_4(s^*)$, $P_5(s^* l^x)$ for $SC(25,24)$ and $P_5(s^*)$, $P_6(s^* l^x)$, $P_7(s^* l^{2x})$ for $SC(9,8)$ with the values of x indicated in the text.

d_{fw} of the Wolff clusters as 1.7525(45) and 1.747(20) for $SC(25,24)$, and $SC(9,8)$ respectively. According to the Fortuin-Kasteleyn mapping [3], $\langle s \rangle_k$ is proportional to the zero field magnetic susceptibility χ; we can check that the value of γ/ν extracted from the behavior of $\chi^{\max}(L)$ and the value of d_{fw} are compatible in the cases of these fractals.

Figure 1 shows the normalized cluster size probability distributions $P_k(s)$ generated by the Wolff algorithm at the critical temperature in the case of $SC(25,24)$ for different values of k. On the way, we notice that the precision is better when calculating an exponent from the susceptibility than from the mean cluster size since the latter distributions are double peaked. $P_k(s)$ is constructed in the same way as an histogram: A number N_b of bins is fixed and $P_k(s)$ is the number of clusters generated by the Wolff algorithm, whose sizes lie within the interval $[s - \Delta s_k/2, s + \Delta s_k/2[$, divided by the total number of Monte Carlo steps; Δs_k is set equal to $\left(l^{kD_f}\right)/N_b$. As already pointed out in the case of Hausdorff dimensions between 2 and 3, $P_k(s)$ at the critical point is invariant under a renormalization of the cluster sizes under the form $s \to s/l^x$ [16]. The data collapses of the distibutions $P_k(s)$ obtained when going from an iteration step k to the next (or the previous) are shown in Figure 2 for the two fractal structures we simulated. The exponent x is calculated from a fit of our data. The scaling property of $P_k(s)$ thus reads as:

$$P_k(s) = P_{k-1}(s/l^x). \tag{2}$$

Let us now show that x is equal to the magnetic eigenexponent y_h associated with one of the two relevant directions of the renormalization flows [18]. According to the renormalization group theory, the scaling behaviors of the reduced temperature $t = T/T_c - 1$ and the external magnetic field h near the criticality under a change of the length unit from 1 to l are described by the two critical eigen-exponents y_t and y_h:

$$t \to t' = l^{y_t} t,$$
$$h \to h' = l^{y_h} h.$$

When a fractal is renormalized from the kth iteration step to the previous one, the lattice size is divided by l, the width Δs_k of the histogram bins and the number of sites N are divided by l^{D_f}. The scaling property described by equation (2) is more conveniently expressed in terms of the Wolff probability density $\mathcal{P}_k(s)$:

$$\mathcal{P}_k(s) = \frac{1}{l^{D_f}} \mathcal{P}_{k-1}(s/l^x). \tag{3}$$

The mean size $\langle s \rangle_k$ of the Wolff clusters at the kth iteration step is related to the mean size at the previous one according to the relation:

$$\langle s \rangle_k = \int_0^{l^{kD_f}} s \mathcal{P}_k(s) \mathrm{d}s = l^{2x - D_f} \int_0^{l^{kD_f - x}} s' \mathcal{P}_{k-1}(s') \mathrm{d}s' \tag{4}$$

where $s' = s/l^x$. Assuming that $x < D_f$ and since we have $\mathcal{P}_{k-1}(s) = 0, \forall s > l^{(k-1)D_f}$, the upper bound of the right side integral can be decreased to $l^{(k-1)D_f}$, and it yields:

$$\langle s \rangle_k = l^{2x - D_f} \langle s \rangle_{k-1}. \tag{5}$$

Since $\langle s \rangle_k$ is proportional to $\left(l^k\right)^{\gamma/\nu}$, it turns out that $2x = D_f + \gamma/\nu$. Assuming that the hyperscaling relation involves the Hausdorff dimension [11], γ/ν is equal

to $2y_h - D_f$. Thus we have $x = y_h$, which can be written $x = \beta/\nu + \gamma/\nu$. The values of x calculated from the scaling of the peaks in $P_k(s)$ and used to plot the data collapses in Figure 2 are 1.857 and 1.82 for $SC(25,24)$ and $SC(9,8)$, respectively; an estimation of the error bars leads to 1.857(6) and 1.82(1). A good agreement with the values of y_h calculated from the finite-size scaling analysis is found, since it yields 1.8608(54) and 1.807(14) for $SC(25,24)$ and $SC(9,8)$, respectively.

The structure of $P_k(s)$ shows that very few clusters of intermediate size are generated at the critical point (the logarithmic scales can be misleading). This effect of segregation between big and large clusters has already been noticed in the translational invariant bidimensionnal case [19] and in the case of Sierpinski fractals [16] with a Hausdorff dimension between 2 and 3. The relative widths $\Delta s/s_{\max}$ of the peaks of the distribution associated with large clusters appear to narrow down as the fractal dimension decreases, since they are equal to 0.21(2) for $SC(25,24)$ and 0.09(1) for $SC(9,8)$; Δs is calculated at the half height measured from the positions of the maximum $s_{\max}$ and the left minimum of the peaks. Thus, this effect of segregation turns out to be all the more pronounced as the fractal dimension is lowered from 2 to 1. As a matter of fact, near the critical point, the lattice is invaded by a low number of big clusters, even a single one, surrounded by several small clusters. An explanation can be provided by looking at the mean behavior of the long range order: The spatial pair correlation function defined as the average $G(r) = \langle S(0)S(r)\rangle$ where r is the distance between two spin $S(0)$ and $S(r)$ is assumed to follow an asymptotic power law decay at the critical point as r tends towards infinity:

$$G(r) \sim \frac{1}{r^{D_f-2+\eta}} \tag{6}$$

η, usually called the anomalous dimension exponent, can be related to γ/ν according to a dimensional analysis [18]: $\eta = 2 - \gamma/\nu$. The asymptotic behavior of $G(r)$ at the critical temperature writes:

$$G(r) \sim \frac{1}{r^{D_f-\gamma/\nu}}\,. \tag{7}$$

The scaling of $G(r)$ with r follows the same power law as the scaling of the ratio of the mean cluster size to the total number of sites of the lattice with its size L:

$$\rho(L) = \frac{\langle s\rangle_k}{L^{D_f}} \sim \frac{1}{L^{D_f-\gamma/\nu}}\,. \tag{8}$$

It can be seen from the last column of Table 1 that $G(r)$ and $\rho(L)$ decay all the slower as the fractal dimension is lowered. Furthermore, $\rho(L)$ tends to 1 as D_f tends towards the lower critical dimension of the Ising model, namely 1, where the transition occurs at $T = 0$ and becomes infinitely narrow. We expect that the effect of invasion of the lattice by a single cluster in the critical region, is all the more important as the fractal dimension is lowered.

4 Dynamics

Whereas the time is a basic parameter in molecular dynamics simulations, the link between the time and a sequence of Monte Carlo steps is much less obvious: The Markov chains generated by the Monte Carlo algorithms can be interpreted in the framework of stochastic kinetics. In this way, several kinetics processes can be defined, according to the chosen algorithm: For instance, single spin-flip kinetics is associated with the Metropolis algorithm, while single cluster kinetics is associated with the Wolff one. There is much to learn in studying the relaxation, that is, how a system is driven to thermal equilibrium. Static critical properties, as well as dynamic ones, can be brought out by annealing [20] or quenching [17] an Ising system on a fractal-like structure to the critical temperature. Let us notice that unfortunately, no quantitative comparisons can be achieved between the results of the two papers quoted above and ours because spins are not placed in the same way on the lattice. Since we want to focus on the critical slowing down, we simulate systems at thermal equilibrium and at the critical temperature; thus, our dynamical study involves the autocorrelation functions defined in Section 2. There are many ways to calculate times from these functions [19], and different physical meanings can be given to them. We deal with the integrated autocorrelation times because they are directly related to the statistical errors associated with the thermal averages; thus they provide a measure of the critical slowing down. Let us recall that the statistical error $\delta\langle E\rangle$ associated with the mean value of the energy $\langle E\rangle$ calculated from a Monte Carlo run of N_S steps can be written as [2]:

$$(\delta\langle E\rangle)^2 \simeq \frac{1}{N_s}\left(\langle E^2\rangle - \langle E\rangle^2\right)\left[1 + 2\frac{\tau_E}{\delta t}\right] \tag{9}$$

where τ_E is the integrated autocorrelation time associated with E, defined as $\tau_E = \int_0^\infty c_E(t)\mathrm{d}t$, $c_E(t)$ being the autocorrelation function in the continuous limit; δt is the unit time associated with one Monte Carlo step. As in the cases of Hausdorff dimensions larger than two [16], we develop $C_E(n)$ (and $C_M(n)$) on a restricted basis of exponential functions:

$$C_E(n) = \sum_{i=1}^{p} a_i \exp\left(-n/\tau_i\right). \tag{10}$$

The integrated autocorrelation times are easily calculated from the fits of the autocorrelation functions according to the relation: $\tau_E = \sum_{i=1}^{p} \tau_i a_i$, with $\sum_{i=1}^{p} a_i = 1$.

4.1 Wolff dynamics

Comparisons between algorithms can be properly achieved only if the time unit is the same. Conventionally, this unit

Table 3. Values of the energy (τ_E^{me}) and magnetization (τ_M^{me}) integrated autocorrelation times measured at different iteration steps k for the Wolff algorithm. The next to last column shows the values of z_w^{me} directly obtained from power law fits, and the last column the values of z_w deduced from the equation (11).

Structure		$k=3$	$k=4$	$k=5$	$k=6$	$k=7$	z_w^{me}	z_w
$SC(25,24)$	τ_M^{me}	3.630(8)	5.45(2)	8.01(15)			0.246(8)	0.0214(130)
$SC(25,24)$	τ_E^{me}	5.650(5)	10.80(7)	19.25(15)			0.377(8)	0.1524(130)
$SC(9,8)$	τ_M^{me}		1.182(2)	1.283(6)	1.335(2)	1.397(3)	0.0387(31)	-0.12
$SC(9,8)$	τ_E^{me}		1.774(2)	2.447(20)	3.155(37)	4.232(8)	0.250(6)	0.089(15)

is the Monte Carlo step per entire lattice update. Since $s(n)$ single spin flips correspond to one Wolff step, the integrated Wolff autocorrelation times τ_E^{me} and τ_M^{me} (per Wolff cluster) measured from the decay of the autocorrelation functions have to be rescaled according to the relation: $\tau_E = \frac{\langle s \rangle_k}{L^{d_f w}} \tau_E^{me}$. If the measured autocorrelation times τ_E^{me} follow a power law at the critical temperature with an exponent z_w^{me}, the Wolff dynamical critical exponent z_w associated with the fractal structure $SC(l^2, N_{occ})$ reads:

$$z_w = z_w^{me} + \frac{\gamma}{\nu} - D_f. \tag{11}$$

The autocorrelation functions have firstly been calculated from each Wolff Monte Carlo run of 10^6 steps at the critical temperatures, and their averages deduced from these 5 results. They have secondly been calculated from a single Wolff Monte Carlo run over 5×10^6 steps. The consistency between the two methods have been checked. Fits under the form given in equation (10) have then been performed from $n = 0$ to a cutoff n_C, and integrated autocorrelation times deduced from the results of the fits; $p = 2$ or $p = 3$ exponential functions yield reliable fits. In the case of the magnetization, we let n_C vary from 50 to 1500 in order to check that the values of τ_M^{me} are stable with respect to n_C. In the case of the energy, the unphysical tails of the autocorrelation functions appear earlier and the maximum value of n_C must be smaller. As a result, the values of the measured integrated autocorrelation times τ_E^{me} and τ_M^{me} with their error bars are reported in Table 3 and the values of the exponents z_w^{me} extracted from power law fits are reported in the next to last column of Table 3. We should point out that, although the fits are performed from a small number of points, these points are distributed over a large range of sizes. The evolution of the rescaled times with L is shown in Figure 3 in logarithmic coordinates. The values of the dynamical exponents z_w, reported in the last column of Table 3, deserve the following comments:

i) The behavior of the energy and the magnetization provide different dynamical exponents; the Wolff algorithm is always more efficient in decorrelating the magnetization. The negative value of $z_w(M)$ in the case of $SC(9,8)$ means that less than an entire lattice update is sufficient to decorrelate M.

ii) The values of the dynamical exponent associated with the slowest quantity, namely $z_w(E)$, are positive (it means that $\tau(E)$ increases with L). Moreover, the Wolff algorithm is all the more efficient in reducing the critical slowing down as the fractal dimension decreases, since $z_w(E)$ decreases with D_f. We should stress that such a conclusion cannot be drawn for structures which share the same fractal dimensions but different generating cells.

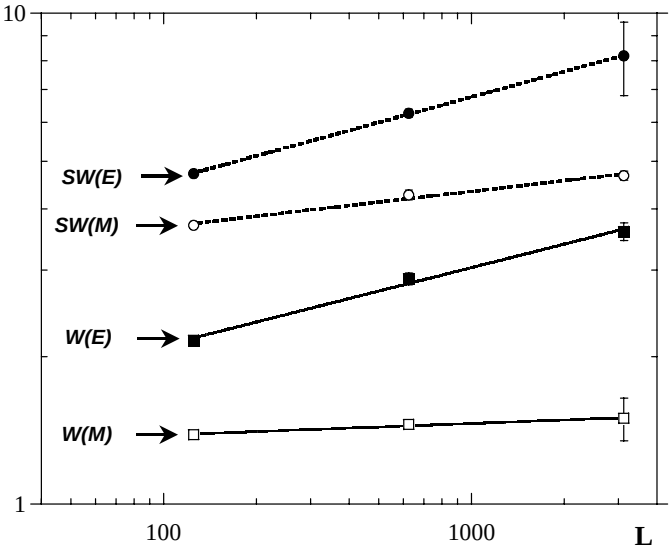

Fig. 3. Integrated autocorrelation times for the Swendsen-Wang algorithm (indicated by $SW(E)$ for the energy and $SW(M)$ for the magnetization) and rescaled times for the Wolff ones ($W(E)$ and $W(M)$) as a function of L for $SC(25,24)$.

4.2 Swendsen-Wang dynamics

The integrated autocorrelation times have been calculated from Swendsen-Wang Monte Carlo simulations performed under the same conditions as the Wolff ones. Since the entire lattice is updated during a Swendsen-Wang Monte Carlo step, there is no need to rescale the measured times; the values of τ_E and τ_M with the error bars are summarized in Table 4. Figure 4 shows their behavior with the lattice size L. The dynamical exponents z_{sw} calculated from power law fits are reported in the last column of Table 4. We should point out that the Swendsen-Wang algorithm share the following features with the Wolff one:

i) The values of $z_{sw}(M)$ are smaller than $z_{sw}(E)$; it remains less difficult to decorrelate the magnetization than

Table 4. Values of the energy (τ_E) and magnetization (τ_M) integrated autocorrelation times measured at different iteration steps k for the Swendsen-Wang algorithm. The last column shows the values of z_{sw} directly obtained from power law fits.

Structure		$k=3$	$k=4$	$k=5$	$k=6$	$k=7$	z_{sw}
$SC(25,24)$	τ_M	3.70(2)	4.27(10)	4.67(10)			0.072(12)
$SC(25,24)$	τ_E	4.72(3)	6.26(12)	8.2(1.4)			0.17(5)
$SC(9,8)$	τ_M		2.16(2)	2.05(3)	1.96(3)	1.84(5)	-0.048
$SC(9,8)$	τ_E		2.48(2)	2.58(4)	2.73(6)	2.77(9)	0.035(20)

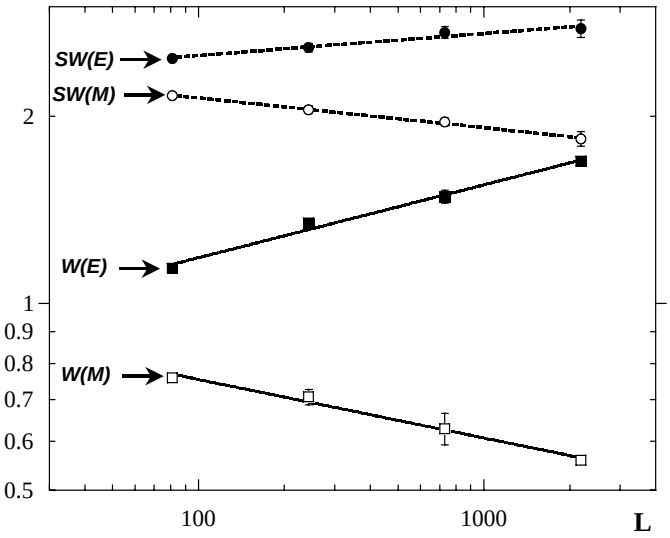

Fig. 4. Integrated autocorrelation times for the Swendsen-Wang algorithm ($SW(E)$ and $SW(M)$) and rescaled times for the Wolff ones ($W(E)$ and $W(M)$) as a function of L for $SC(9,8)$.

the energy. The negative value of $z_{sw}(M)$ in the case of $SC(9,8)$ confirms that less than an entire lattice update is sufficient to decorrelate M.

ii) The values of the exponent associated with the slowest physical quantity, namely $z_{sw}(E)$ are positive and decrease with D_f.

Moreover, the comparison between the efficiency of the algorithms in reducing the critical slowing down can be conveniently achieved by looking at Figures 3 and 4: the rescaled autocorrelation times for the Wolff algorithm and the autocorrelation times for the Swendsen-Wang ones are plotted together as a function of L. It turns out that Wolff is always more efficient in the range of sizes we studied. Nevertheless a kind of crossover seems to arise in the case of $SC(9,8)$, where Swendsen-Wang should be more efficient in decorrelating the energy when the size L becomes very large (about $L > 3^{13}$). We should mention than the rigourous Li-Sokal lower bound α/ν for the Swendsen-Wang algorithm [21] holds in the case of the fractal structures we studied (since α is negative).

A part of the numerical simulations has been carried out in the Institut de Développement et des Ressources en Informatique Scientifique (IDRIS), supported by the Centre National de la Recherche Scientifique (project number 021186). We acknowledge the scientific committee and the staff of the center. We are also grateful to the Centre de Calcul Recherche (CCR) of the University Paris VII Denis Diderot, where the rest of the simulations have been done.

References

1. Y. Gefen, B.B. Mandelbrot, A. Aharony, Phys. Rev. Lett. **45**, 855 (1980)
2. K. Binder, D.W. Heermann in *Monte Carlo simulation in Statistical Physics* (Springer-Verlag, Berlin, Heidelberg, New-York, 1988)
3. C.M. Fortuin, P.W. Kasteleyn, Physica A **57**, 536 (1972)
4. R.H. Swendsen, J.S. Wang, Phys. Rev. Lett. **58**, 86 (1987)
5. U. Wolff, Phys. Rev. Lett. **62**, 361 (1989)
6. A.M. Ferrenberg, R.H. Swendsen, Phys. Rev. Lett. **61**, 2635 (1988)
7. A.M. Ferrenberg, R.H. Swendsen, Phys. Rev. Lett. **63**, 1195 (1989)
8. P. Monceau, M. Perreau, F. Hébert, Phys. Rev. B **58**, 6386 (1998)
9. J. Carmona, U.M.B. Marconi, J.J. Ruiz-Lorenzo, A. Tarancón, Phys. Rev. B **58**, 14387 (1998)
10. P.Y. Hsiao, P. Monceau, M. Perreau, Phys. Rev. B **63**, 13856 (2000)
11. P. Monceau, M. Perreau, Phys. Rev. B **63**, 184420 (2001)
12. P. Monceau, P.Y. Hsiao, Phys. Lett. A **300**, 685 (2002)
13. J.C. Le Guillou, J. Zinn-Justin, J. Phys. **48**, 19 (1987)
14. Y. Gefen, A. Aharony, B.B. Mandelbrot, J. Phys. A Math. Gen. **17**, (1984)
15. Y.K. Wu, B. Hu, Phys. Rev. A **35**, 1404 (1987)
16. P. Monceau, P.Y. Hsiao, Phys. Rev. B **66**, 104422 (2002)
17. G.P. Zheng, M. Li, Phys. Rev. B **62**, 6253 (2000)
18. J.J. Binney, N.J. Dowrick, A.J. Fisher, M.E.J. Newman, in *The Theory of Critical Phenomena* (Oxford University Press, 1992)
19. P. Tamayo, R.C. Brower, W. Klein, J. Stat. Phys. **58**, 1083 (1990)
20. G. Pruessner, D. Loison, K.D. Schotte, Phys. Rev. B **64**, 134414 (2001)
21. X.J. Li, A.D. Sokal, Phys. Rev. Lett. **63**, 827 (1989)